Available online at www.sciencedirect.com
ScienceDirect
Journal of Sound and Vibration 310 (2008) 421–432
JOURNAL OF SOUND AND VIBRATION
www.elsevier.com/locate/jsvi

Vibration isolation using buckled or pre-bent columns—Part 2: Three-dimensional motions of horizontal rigid plate

A.E. Jeffers[a], R.H. Plaut[a,*], L.N. Virgin[b]

[a]*The Charles E. Via, Jr., Department of Civil and Environmental Engineering, Virginia Polytechnic Institute and State University, Blacksburg, VA 24061-0105, USA*

[b]*Department of Civil and Environmental Engineering, Duke University, Durham, NC 27708-0287, USA*

Accepted 25 September 2007
The peer review of this article was organised by the Guest Editor
Available online 5 November 2007

Abstract

This is a continuation of previous work to investigate the use of pairs of pre-bent columns, bonded with a viscoelastic filler, as vibration isolators. In this paper, four of these devices support the corners of a square, rigid plate. When the system is in equilibrium, small harmonic vibrations are applied vertically to the base of the isolators, and the steady-state response of the system is determined. First, the system is analyzed for the fully symmetric case, i.e., the center of mass of the plate coincides with the geometric center. Then, the system is analyzed for various cases in which the center of mass has some eccentricity. The eccentric weight introduces rotational motions of the plate. The governing equations are formulated and then numerically solved in Mathematica using a shooting method. The displacement transmissibility is plotted over a range of excitation frequencies, and the mode shapes are shown for the first few resonant frequencies. Free vibration of the system is also considered. For this three-dimensional system, the pre-bent columns can be effective at isolating vibrations for a wide range of excitation frequencies.

1. Introduction

Plaut et al. [1] considered the use of buckled columns and pre-bent columns as vibration isolators in a two-dimensional (2D) system subjected to simple-harmonic base excitation. The system consisted of a rigid bar supported at either end by buckled or pre-bent columns. For the case in which the bar was supported by buckled columns, the bar was allowed to have an asymmetric shape and then exhibited rotational as well as translational motion. The analysis considered the effect of this asymmetry on the efficiency of the vibration isolators. For the case in which a symmetric bar was supported by pairs of pre-bent columns, the paper examined the effects of various filler stiffnesses, axial loads, and initial curvatures on the displacement transmissibility. Ref. [1] contains a review of the literature pertaining to the use of buckled and pre-bent

*Corresponding author. Tel.: +1 540 231 6072; fax: +1 540 231 7532.
E-mail address: rplaut@vt.edu (R.H. Plaut).

0022-460X/$ - see front matter © 2007 Elsevier Ltd. All rights reserved.
doi:10.1016/j.jsv.2007.09.039

columns as vibration isolators. Such devices may be able to support heavy loads statically without large vertical deflections, and then be effective in absorbing dynamic base excitations.

The present analysis extends previous work by considering pre-bent columns as vibration isolators in a system that incorporates three-dimensional (3D) motions of a horizontal rigid plate. The plate is allowed to move in the vertical direction and rotate about two horizontal axes. Under simple-harmonic base excitation, the steady-state response of the system is analyzed. The efficiency of the isolators is considered for various cases, including the fully symmetric case. Free vibrations of the system also are investigated.

2. Formulation

2.1. Variables and parameters

The system shown in Fig. 1 consists of a square, rigid plate supported at each corner by a pair of pre-bent columns. The plate is nonuniform such that the center of mass of its weight occurs at some distance from the geometric center of the plate. Despite this nonuniformity, the bottom of the plate is assumed to be flat. The location of the plate's center of mass is indicated by the dimensions A_1, A_2, B_1, and B_2, and the center of mass occurs at a vertical distance H from the bottom of the plate. The plate has mass moments of inertia I_x and I_y about lines through the center of mass and parallel to the $\bar{X}$ and $\bar{Y}$ axes, respectively. This system could represent, for example, a table with equipment mounted on it. (Tang et al. [2] used a similar model to investigate the 3D motions of a hydraulic platform subjected to an impulsive load.)

The $\bar{X}$, $\bar{Y}$, $\bar{Z}$ coordinate system is fixed in space with its origin at the base of isolator 1 and has unit vectors $\hat{i}$, $\hat{j}$, and $\hat{k}$. Angles θ, ψ, and ϕ are used to define rotations about the $\bar{X}$, $-\bar{Y}$, and $\bar{Z}$ axes, respectively, and are initially zero. When the system is in equilibrium, the bottom of the plate is assumed to be perfectly horizontal, i.e., all four isolators have the same initial height H_0. This is achieved by adjusting the width of each column in isolator j by a factor α_j. Under dynamic excitation, the center of mass of the plate moves from its equilibrium position with displacements $X(T)$, $Y(T)$, and $Z(T)$, where T denotes time, and the plate rotates with angles $\theta(T)$ and $\psi(T)$ about the $\bar{X}$ and $-\bar{Y}$ axes, respectively. Rotation $\phi(T)$ about the $\bar{Z}$-axis is restrained. It is assumed that the system is braced laterally so as to prohibit sway and prevent collapse. A simple-harmonic vertical displacement $U(T)$ is imposed at the base of each isolator and is defined as $U(T) = U_0 \sin \Omega T$, where U_0 is the amplitude of the motion and Ω is the excitation frequency.

Each isolator is attached to a corner of the plate with a spherical joint that transfers no moment. To account for the resistance of the system to horizontal motions of the plate, horizontal springs are attached to the

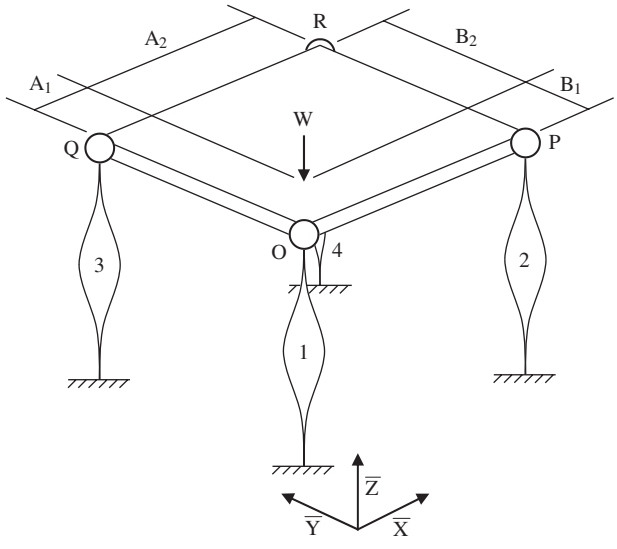

Fig. 1. Model of the rigid plate supported by pre-bent columns.

corners of the plate, as shown in Fig. 2. Spring n is assumed to have stiffness K_n. Because of these stiff springs, and because only small rotations of the plate are considered, the horizontal movement at the top of each isolator will be extremely small. Therefore it can be assumed that the two columns of each isolator move as mirror images of each other about a vertical line through its center, and symmetry can be utilized in the analysis of the isolator.

Fig. 3 shows isolator j in a horizontal configuration. The two columns in isolator j are clamped at both ends, and the viscoelastic filler is bonded to the inner sides of the two columns. Because of the assumed symmetry, both columns in isolator j behave identically and so only the upper column is described. It is treated as an inextensible elastica. The column is uniform and has constant bending stiffness $\alpha_j EI_c$ and mass per unit length $\alpha_j \mu$. The motion of the column is defined in terms of the arc length S_j, the angle of rotation $\theta_j(S_j, T)$, and the axial and transverse coordinates $X_j(S_j, T)$ and $Y_j(S_j, T)$, respectively. The filler has distributed stiffness and damping, which are shown in Fig. 3 as a series of springs and dashpots along the length of the isolator.

Before any load is applied to the isolator, each column has an initial pre-bent shape defined by the angle

$$\theta_0(S_j) = d_0 \sin\left(\frac{2\pi S_j}{L}\right) \tag{1}$$

which corresponds to an initial horizontal deflection $Y_0(S_j)$ in Fig. 3. It is assumed that the column and filler are unstrained when the column is in this initial configuration. An axial load $F_j(T)$ is transmitted from the corner of the plate to the top of isolator j. The column has axial force $P_j(S_j,T)$, transverse force $Q_j(S_j,T)$, and bending moment $M_j(S_j,T)$. The filler resists the deformation due to axial load $F_j(T)$ and base excitation $U(T)$ with forces due to the filler stiffness and damping, as described in Ref. [1] and involving a stiffness coefficient K_f and a damping coefficient C_f. It is assumed that the filler does not provide stiffness or damping in the axial direction. A free body diagram of element dS_j of the column, including inertia and damping forces, is shown in Fig. 4.

2.2. Equations for the isolator

Small steady-state motions of the column about equilibrium are considered under the harmonic base excitation $U(T)$. From equilibrium, geometry, and the constitutive law for the column in isolator j, the

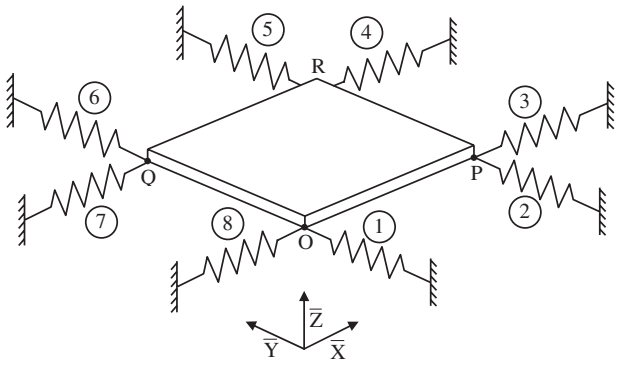

Fig. 2. Rigid plate and horizontal springs.

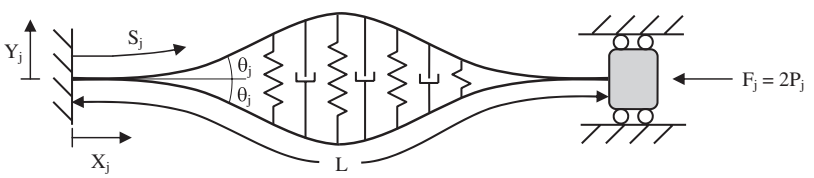

Fig. 3. Vibration isolator j under axial load F_j.

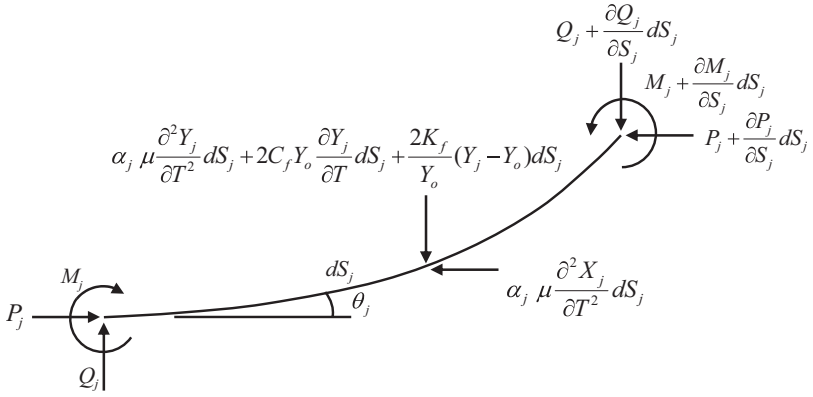

Fig. 4. Free body diagram of column element, including inertia and damping forces.

governing equations are [1]

$$\frac{\partial X_j}{\partial S_j} = \cos\,\theta_j, \quad \frac{\partial Y_j}{\partial S_j} = \sin\,\theta_j, \quad \frac{\partial \theta_j}{\partial S_j} = \frac{M_j}{\alpha_j \mathrm{EI}_c} + \frac{2\pi}{L} d_0 \cos\left(\frac{2\pi S_j}{L}\right),$$
$$\frac{\partial M_j}{\partial S_j} = -P_j \sin\,\theta_j + Q_j \cos\,\theta_j,$$
$$\frac{\partial P_j}{\partial S_j} = -\alpha_j \mu \frac{\partial^2 X_j}{\partial T^2}, \quad \frac{\partial Q_j}{\partial S_j} = -\alpha_j \mu \frac{\partial^2 Y_j}{\partial T^2} - 2C_f Y_0 \frac{\partial Y_j}{\partial T} - \frac{2K_f}{Y_0}(Y_j - Y_0) \quad (j = 1, 2, 3, 4). \tag{2}$$

For steady-state motions, the column variables can be written in the complex form of Eqs. (2) in Ref. [1], except that here Q_{je} is a function of S_j and j goes from 1 to 4. For equilibrium, the first, second, and fourth of Eqs. (3) in Ref. [1] are valid for j from 1 to 4, and also

$$\frac{\mathrm{d}\theta_{je}}{\mathrm{d}S_j} = \frac{M_{je}}{\alpha_j EI_c} + \frac{2\pi}{L} d_0 \cos\left(\frac{2\pi S_j}{L}\right), \quad \frac{\mathrm{d}Q_{je}}{\mathrm{d}S_j} = \frac{-2K_f}{Y_0}(Y_{je} - Y_0) \quad (j = 1, 2, 3, 4). \tag{3}$$

The subscript "e" designates equilibrium quantities and the subscript "d" indicates dynamic quantities.

The linear equations for the dynamic variables are given by the first four of Eqs. (4) in Ref. [1] for j from 1 to 4, along with

$$\frac{\mathrm{d}P_{jd}}{\mathrm{d}S_j} = \alpha_j \mu \Omega^2 X_{jd}, \quad \frac{\mathrm{d}Q_{jd}}{\mathrm{d}S_j} = \left[\alpha_j \mu \Omega^2 - \mathrm{i}\Omega(2C_f Y_0) - \frac{2K_f}{Y_0}\right] Y_{jd} \quad (j = 1, 2, 3, 4). \tag{4}$$

2.3. Equations for the rigid plate

The position vectors from the origin of the fixed $\bar{X}$, $\bar{Y}$, $\bar{Z}$ coordinate system to the corners O, P, Q, and R of the plate during dynamic excitation can be written as

$$\bar{r}_O(T) = X_O(T)\hat{i} + Y_O(T)\hat{j} + Z_O(T)\hat{k}, \quad \bar{r}_P(T) = X_P(T)\hat{i} + Y_P(T)\hat{j} + Z_P(T)\hat{k},$$
$$\bar{r}_Q(T) = X_Q(T)\hat{i} + Y_Q(T)\hat{j} + Z_Q(T)\hat{k}, \quad \bar{r}_R(T) = X_R(T)\hat{i} + Y_R(T)\hat{j} + Z_R(T)\hat{k}, \tag{5}$$

where the components of vectors $\bar{r}_O(T)$, $\bar{r}_P(T)$, $\bar{r}_Q(T)$, and $\bar{r}_R(T)$ are written in terms of the displacements $X(T)$, $Y(T)$, and $Z(T)$ and rotations $\theta(T)$ and $\psi(T)$ as

$$X_O(T) = X(T) + A_1 - A_1 \cos\psi(T) + H \sin\psi(T),$$
$$X_P(T) = X(T) + A_1 + A_2 \cos\psi(T) + H \sin\psi(T),$$

$$
\begin{aligned}
X_Q(T) &= X(T) + A_1 - A_1\cos\psi(T) + H\sin\psi(T),\\
X_R(T) &= X(T) + A_1 + A_2\cos\psi(T) + H\sin\psi(T),\\
Y_O(T) &= Y(T) + B_1 + A_1\sin\psi(T)\sin\theta(T) - B_1\cos\theta(T) + H\cos\psi(T)\sin\theta(T),\\
Y_P(T) &= Y(T) + B_1 - A_2\sin\psi(T)\sin\theta(T) - B_1\cos\theta(T) + H\cos\psi(T)\sin\theta(T),\\
Y_Q(T) &= Y(T) + B_1 + A_1\sin\psi(T)\sin\theta(T) + B_2\cos\theta(T) + H\cos\psi(T)\sin\theta(T),\\
Y_R(T) &= Y(T) + B_1 - A_2\sin\psi(T)\sin\theta(T) + B_2\cos\theta(T) + H\cos\psi(T)\sin\theta(T),\\
Z_O(T) &= Z(T) + H_0 + H - A_1\sin\psi(T)\cos\theta(T) - B_1\sin\theta(T) - H\cos\psi(T)\cos\theta(T),\\
Z_P(T) &= Z(T) + H_0 + H + A_2\sin\psi(T)\cos\theta(T) - B_1\sin\theta(T) - H\cos\psi(T)\cos\theta(T),\\
Z_Q(T) &= Z(T) + H_0 + H - A_1\sin\psi(T)\cos\theta(T) + B_2\sin\theta(T) - H\cos\psi(T)\cos\theta(T),\\
Z_R(T) &= Z(T) + H_0 + H + A_2\sin\psi(T)\cos\theta(T) + B_2\sin\theta(T) - H\cos\psi(T)\cos\theta(T).
\end{aligned}
\tag{6}
$$

From Eqs. (6), the angles $\theta(T)$ and $\psi(T)$ are related to the displacements at the corners of the plate by

$$
\begin{aligned}
\sin\theta(T) &= \frac{Z_R(T) - Z_P(T)}{B_1 + B_2} = \frac{Z_Q(T) - Z_O(T)}{B_1 + B_2},\\
\sin\psi(T) &= \frac{Z_R(T) - Z_Q(T)}{A_1 + A_2} = \frac{Z_P(T) - Z_O(T)}{A_1 + A_2},\\
\cos\theta(T) &= \frac{Y_R(T) - Y_P(T)}{B_1 + B_2} = \frac{Y_Q(T) - Y_O(T)}{B_1 + B_2},\\
\cos\psi(T) &= \frac{X_R(T) - X_Q(T)}{A_1 + A_2} = \frac{X_P(T) - X_O(T)}{A_1 + A_2}.
\end{aligned}
\tag{7}
$$

The equations of motion for the plate are [3]

$$
\begin{aligned}
&M\frac{\mathrm{d}^2X(T)}{\mathrm{d}T^2} + (K_3 + K_4)[X(T) + A_2\cos\psi(T) - A_2 + H\sin\psi(T)]\\
&\quad + (K_7 + K_8)[X(T) + A_1 - A_1\cos\psi(T) + H\sin\psi(T)] = 0,
\end{aligned}
\tag{8}
$$

$$
\begin{aligned}
&M\frac{\mathrm{d}^2Y(T)}{\mathrm{d}T^2} + (K_1 + K_2)[Y(T) + B_1 - B_1\cos\theta(T) + H\sin\theta(T)]\\
&\quad + (K_5 + K_6)[Y(T) + B_2\cos\theta(T) - B_2 + H\sin\theta(T)] = 0,
\end{aligned}
\tag{9}
$$

$$
M\frac{\mathrm{d}^2Z(T)}{\mathrm{d}T^2} = F_1(T) + F_2(T) + F_3(T) + F_4(T) - W,
\tag{10}
$$

$$
\begin{aligned}
&I_x\frac{\mathrm{d}^2\theta(T)}{\mathrm{d}T^2} + (K_1 + K_2)[Y(T) + B_1 - B_1\cos\theta(T) + H\sin\theta(T)][H\cos\theta(T) + B_1\sin\theta(T)]\\
&\quad + (K_5 + K_6)[Y(T) + B_2\cos\theta(T) - B_2 + H\sin\theta(T)][H\cos\theta(T) - B_2\sin\theta(T)]\\
&\quad = -[F_1(T) + F_2(T)]B_1 + [F_3(T) + F_4(T)]B_2,
\end{aligned}
\tag{11}
$$

$$
\begin{aligned}
&I_y\frac{\mathrm{d}^2\psi(T)}{\mathrm{d}T^2} + (K_3 + K_4)[X(T) + A_2\cos\psi(T) - A_2 + H\sin\psi(T)][H\cos\psi(T) - A_2\sin\psi(T)]\\
&\quad + (K_7 + K_8)[X(T) + A_1 - A_1\cos\psi(T) + H\sin\psi(T)][H\cos\psi(T) + A_1\sin\psi(T)]\\
&\quad = -[F_1(T) + F_3(T)]A_1 + [F_2(T) + F_4(T)]A_2,
\end{aligned}
\tag{12}
$$

where M is the mass of the plate. From geometry,

$$
X(T) = X_O(T) - A_1 + \frac{A_1}{A_1 + A_2}[X_P(T) - X_O(T)] - \frac{H}{A_1 + A_2}[Z_P(T) - Z_O(T)],
\tag{13}
$$

$$Y(T) = Y_O(T) - B_1 + \frac{B_1}{B_1 + B_2}[Y_Q(T) - Y_O(T)] - \frac{H}{B_1 + B_2}[Z_Q(T) - Z_O(T)], \tag{14}$$

$$Z(T) = Z_O(T) - H_O - H + \frac{A_1}{A_1 + A_2}[Z_P(T) - Z_O(T)] + \frac{B_1}{B_1 + B_2}[Z_Q(T) - Z_O(T)] + H\frac{[X_P(T) - X_O(T)][Y_Q(T) - Y_O(T)]}{(A_1 + A_2)(B_1 + B_2)}. \tag{15}$$

For steady-state motions, the coordinates of the corners O, P, Q, and R can be written as

$$\begin{aligned}
&X_O(T) = X_{Od}\,e^{i\Omega T}, \quad X_P(T) = A_1 + A_2 + X_{Pd}\,e^{i\Omega T}, \quad X_Q(T) = X_{Qd}\,e^{i\Omega T},\\
&X_R(T) = A_1 + A_2 + X_{Rd}\,e^{i\Omega T}, \quad Y_O(T) = Y_{Od}\,e^{i\Omega T}, \quad Y_P(T) = Y_{Pd}\,e^{i\Omega T},\\
&Y_Q(T) = B_1 + B_2 + Y_{Qd}\,e^{i\Omega T}, \quad Y_R(T) = B_1 + B_2 + Y_{Rd}\,e^{i\Omega T}, \quad Z_O(T) = H_0 + X_{1d}(L)\,e^{i\Omega T},\\
&Z_P(T) = H_0 + X_{2d}(L)\,e^{i\Omega T}, \quad Z_Q(T) = H_0 + X_{3d}(L)\,e^{i\Omega T}, \quad Z_R(T) = H_0 + X_{4d}(L)\,e^{i\Omega T}
\end{aligned} \tag{16}$$

and the axial force for isolator j is written in terms of the column force as

$$F_j(T) = 2P_{je} + 2P_{jd}\,e^{i\Omega T} \quad (j = 1, 2, 3, 4). \tag{17}$$

Using Eqs. (7) and (13)–(17) in Eqs. (8)–(12), the equations of motion for the plate are written in terms of the column variables and the displacements at the corners of the plate instead of in terms of the displacements and rotations at the center of mass of the plate.

2.4. Boundary conditions, transmissibility, and nondimensional variables

The boundary conditions at the base of isolator j (i.e., at $S_j = 0$) are $X_{je}(0) = 0$, $Y_{je}(0) = 0$, $\theta_{je}(0) = 0$, $X_{jd}(0) = U_0$, $Y_{jd}(0) = 0$, and $\theta_{jd}(0) = 0$ ($j = 1, 2, 3, 4$). At the top of the isolator (i.e., at $S_j = L$), the boundary conditions for the equilibrium variables are

$$\begin{aligned}
&Y_{je}(L) = 0, \quad \theta_{je}(L) = 0, \quad P_{1e} + P_{2e} + P_{3e} + P_{4e} = \frac{W}{2}, \quad (P_{1e} + P_{2e})B_1 - (P_{3e} + P_{4e})B_2 = 0,\\
&(P_{1e} + P_{3e})A_1 - (P_{2e} + P_{4e})A_2 = 0, \quad X_{1e}(L) - X_{2e}(L) - X_{3e}(L) + X_{4e}(L) = 0
\end{aligned} \tag{18}$$

and the boundary conditions for the dynamic variables are

$$\begin{aligned}
&Y_{jd}(L) = 0, \quad \theta_{jd}(L) = 0, \quad X_{1d}(L) - X_{2d}(L) - X_{3d}(L) + X_{4d}(L) = 0,\\
&-\frac{M\Omega^2}{A_1 + A_2}[A_1X_{Pd} + A_2X_{Od} - HX_{2d}(L) + HX_{1d}(L)] + (K_3 + K_4)X_{Pd} + (K_7 + K_8)X_{Od} = 0,\\
&-\frac{M\Omega^2}{B_1 + B_2}[B_1Y_{Qd} + B_2Y_{Od} - HX_{3d}(L) + HX_{1d}(L)] + (K_1 + K_2)Y_{Od} + (K_5 + K_6)Y_{Qd} = 0,\\
&-\frac{M\Omega^2}{A_1 + A_2}[A_1X_{2d}(L) + A_2X_{1d}(L) + HX_{Pd} - HX_{Od}]\\
&\quad -\frac{M\Omega^2}{B_1 + B_2}[B_1X_{3d}(L) - B_1X_{1d}(L) + HY_{Qd} - HY_{Od}] = 2(P_{1d} + P_{2d} + P_{3d} + P_{4d}),\\
&-\frac{I_x\Omega^2}{B_1 + B_2}[X_{3d}(L) - X_{1d}(L)] = -2(P_{1d} + P_{2d})B_1 + 2(P_{3d} + P_{4d})B_2,\\
&-\frac{I_y\Omega^2}{A_1 + A_2}[X_{2d}(L) - X_{1d}(L)] = -2(P_{1d} + P_{3d})A_1 + 2(P_{2d} + P_{4d})A_2.
\end{aligned} \tag{19}$$

Two additional conditions are required to solve for the horizontal displacements at the plate corners. These conditions, derived from geometry, are $Y_{Od} = Y_{Qd}$ and $X_{Od} = X_{Pd}$.

The transmissibility for the system is calculated as the ratio of the average vertical movement of the plate to the amplitude of the base excitation. In terms of the vertical motions at the top of each isolator,

the transmissibility is computed as

$$TR = \frac{1}{4U_0}\sum_{j=1}^{4}\sqrt{\{\mathrm{Re}\,[X_{jd}(L)]\}^2 + \{\mathrm{Im}\,[X_{jd}(L)]\}^2}. \tag{20}$$

Note that the transmissibility is independent of the amplitude U_0, since X_{jd} is proportional to U_0. Calculations are performed in terms of the following nondimensional quantities:

$$a_1 = \frac{A_1}{A_1+A_2}, \quad a_2 = \frac{A_2}{A_1+A_2}, \quad b_1 = \frac{B_1}{A_1+A_2}, \quad b_2 = \frac{B_2}{A_1+A_2}, \quad h = \frac{H}{A_1+A_2}, \quad l = \frac{L}{A_1+A_2},$$
$$h_0 = \frac{H_0}{A_1+A_2}, \quad u_0 = \frac{U_0}{A_1+A_2}, \quad x_{Od} = \frac{X_{Od}}{A_1+A_2}, \quad x_{Pd} = \frac{X_{Pd}}{A_1+A_2}, \quad y_{Od} = \frac{Y_{Od}}{A_1+A_2},$$
$$y_{Qd} = \frac{Y_{Qd}}{A_1+A_2}, \quad s_j = \frac{S_j}{A_1+A_2}, \quad x_j = \frac{X_j}{A_1+A_2}, \quad y_j = \frac{Y_j}{A_1+A_2}, \quad p_j = \frac{P_j(A_1+A_2)^2}{\mathrm{EI}_c},$$
$$q_j = \frac{Q_j(A_1+A_2)^2}{\mathrm{EI}_c}, \quad m_j = \frac{M_j(A_1+A_2)}{\mathrm{EI}_c}, \quad w = \frac{W(A_1+A_2)^2}{\mathrm{EI}_c}, \quad m = \frac{W}{\mu g L},$$
$$k_f = \frac{2K_f(A_1+A_2)^3}{\mathrm{EI}_c}, \quad c_f = \frac{2C_f(A_1+A_2)^3}{\sqrt{\mu \mathrm{EI}_c}}, \quad \omega = \Omega\sqrt{\frac{\mu L^4}{\mathrm{EI}_c}}, \quad t = T\sqrt{\frac{\mathrm{EI}_c}{\mu L^4}},$$
$$k_n = \frac{K_n(A_1+A_2)^3}{\mathrm{EI}_c} \quad (j = 1,2,3,4), \quad (n = 1,2,\ldots,8). \tag{21}$$

The system is first analyzed in equilibrium and then under dynamic excitation. This analysis is conducted in Mathematica [4] using a shooting method to solve the governing equations for the plate and isolators. In the following numerical examples:

$$a_1 + a_2 = b_1 + b_2 = l = 1, \quad h = 0.1375, \quad d_0 = 0.1, \quad k_f = 0.1,$$
$$k_n = 0.1 \quad (n = 1,2,\ldots,8). \tag{22}$$

In addition, the nondimensional weight w is assigned a value of 320 so that the axial force p_{je} in each column for the fully symmetric case is just above the nondimensional critical buckling load for a column that is clamped at both ends. When the plate's center of mass is located eccentrically, the actual load applied to an individual column may be higher or lower than this load. This type of isolator does not need to be loaded above its buckling load to be effective.

3. Results

The system is analyzed for various locations of the center of mass, which are grouped in categories based on the degree of symmetry that exists in the system. These categories are defined as follows:

Case A: This is the fully symmetric case, in which the center of mass is positioned at the geometric center of the plate (i.e., $a_1 = b_1 = 0.5$).

Case B: The center of mass is positioned at points along a line which runs perpendicularly to edge OQ of the plate and passes through the center of the plate (i.e., b_1 is fixed at 0.5).

Case C: The center of mass is positioned at points along a line which runs diagonally from corner O to corner R of the plate (i.e., $a_1 = b_1$).

Case D: The center of mass is positioned such that no symmetry exists in the system.

First, a free vibration analysis of the system is carried out for each of these cases to determine the resonant vibration modes for the plate and to estimate the frequencies at which these vibration modes occur. Then, the forced vibration analysis is performed using the imposed base excitation $U(T)$. In the forced vibration analysis, the transmissibility is calculated and plotted over a range of nondimensional excitation frequencies. At some of the resonant frequencies, the vibration mode shapes are shown for the system.

3.1. Free vibration analysis

For the free vibration analysis, the filler damping coefficient c_f and the amplitude of the base displacement u_0 are set equal to zero. The linearized, undamped, unforced equations of motion are numerically solved in Mathematica. The shooting method is used to determine the unknown parameters, including the frequencies for the vibration modes of the plate. The plate has essentially three degrees of freedom and is expected to have one mode that is dominated by vertical motion and two modes that correspond to distinct rotations.

For the symmetric case (Case A), the plate exhibits a large vertical displacement at the first vibration frequency, $\omega = 0.922$. At the second vibration frequency, $\omega = 1.757$, the plate has rotational vibration modes about *all* lines that pass through the center of the plate, as illustrated by lines A–A', B–B', C–C', and D–D' in Fig. 5(a). In other words, the symmetric system has an infinite number of rotational modes at this frequency. This occurs because of the inherent symmetries that exist in the fully symmetric system. It can be shown by a similar example with vertical springs at the corners [3] that this behavior is expected for such a system.

For Cases B–D, the plate exhibits one mode that is dominated by vertical motion and two rotational modes, each of which corresponds to a distinct frequency that depends on the specific location of the center of mass. For Case B, the rotational modes are characterized by lines A–A' and B–B' in Fig. 5(b). Note that line B–B' is the line of symmetry for this case, and line A–A' is perpendicular to line B–B'. For Case C, the rotational modes are characterized by lines A–A' and B–B' in Fig. 5(c). This time, the line of symmetry, B–B', runs from corner O to corner R, and line A–A' is again perpendicular to B–B'. For Case D, the two rotational modes correspond to two nodal lines that are almost perpendicular to each other, and the positions of these lines are unique for each location of the center of mass because of the lack of symmetry.

3.2. Forced vibration analysis

For the forced vibration analysis, the damping parameter c_f is set equal to unity and the amplitude u_0 of the base displacement (which does not affect the transmissibility) is set equal to 0.001. For each case, the transmissibility is calculated and plotted for a range of nondimensional excitation frequencies. The isolators can be considered effective for ranges of frequencies in which the transmissibility is less than unity. At frequencies where the transmissibility is greater than unity, the base motion is amplified. Peaks in the transmissibility curves indicate resonances.

The transmissibility curve for the symmetric system (Case A) is shown in Fig. 6 for $0.1 < \omega < 100$. The plate does not exhibit rotation in this case. There are three distinct peaks in transmissibility, which occur at frequencies $\omega_1 = 0.922$, $\omega_2 = 44.48$, and $\omega_3 = 78.53$. Between peaks, there are significant ranges of frequencies where the transmissibility is well below unity. The magnitude of the transmissibility at some of the peaks is extremely high (e.g., 2250 at ω_1). This occurs because the filler was assumed to be the only source of damping in the system and the value $c_f = 1$ corresponds to very small damping.

The resonant vibration modes for Case A are shown in Fig. 7 for the first three peak frequencies. Note that these are plots of the dynamic portion y_{jd} of the transverse deflection of the columns. Because of symmetry, the columns in all four isolators behave the same, and so only one column is shown. The first mode shown in Fig. 7(a) corresponds to a large vertical displacement of the plate. At the second and third peak frequencies,

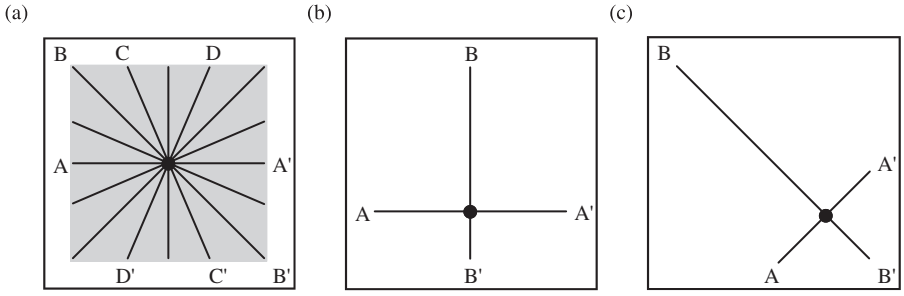

Fig. 5. Characteristic nodal lines for free vibration of (a) Case A, (b) Case B and (c) Case C.

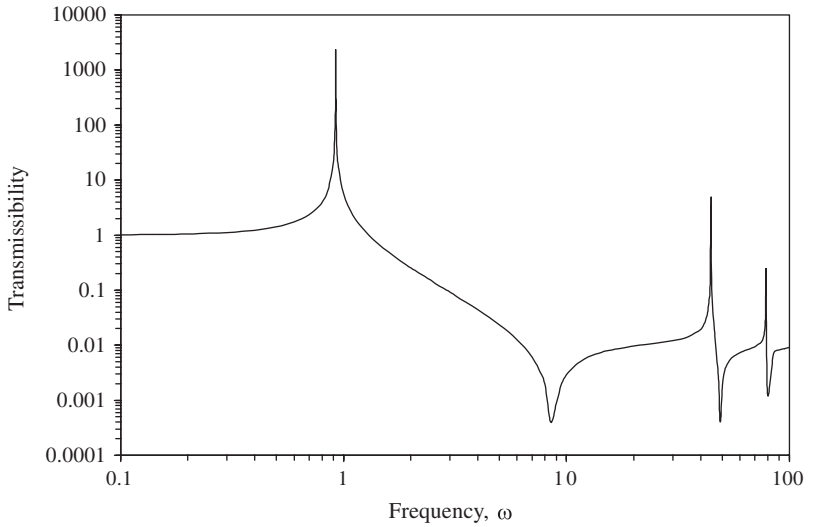

Fig. 6. Transmissibility curve for symmetric case (Case A): $a_1 = 0.50$, $b_1 = 0.50$, $0.1 < \omega < 100$.

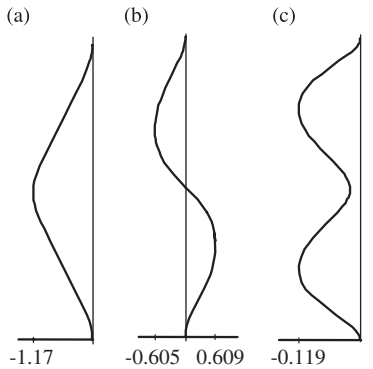

Fig. 7. Steady-state vibration mode shapes for column at peak frequencies for Case A: (a) $\omega = 0.922$, (b) $\omega = 44.48$, and (c) $\omega = 78.53$.

the plate does not exhibit significant vertical movement ($x_{jd}(l) = 0.004$ at ω_2, and $x_{jd}(l) = 0.0002$ at ω_3), but the columns in the isolators demonstrate distinct vibration modes with large transverse deflections, as shown in Figs. 7(b) and (c).

Transmissibility curves are shown in Figs. 8–10 for examples from Cases B–D, respectively. The result from Fig. 6 is included as a dashed curve for comparison. In these examples, the position of the center of mass and values for the mass moments of inertia are $a_1 = 0.35$, $b_1 = 0.50$, $i_x = 22.11$, and $i_y = 27.57$ for Case B, $a_1 = b_1 = 0.35$ and $i_x = i_y = 27.57$ for Case C, and $a_1 = 0.35$, $b_1 = 0.45$, $i_x = 22.72$, and $i_y = 27.57$ for Case D. In the three cases shown in Figs. 8–10, the transmissibility curves have the same general shape as the transmissibility curve for the symmetric case. The most notable difference is that an additional peak appears for Cases B and C, and two additional peaks appear for Case D. These peaks occur at frequencies slightly higher than the first resonant frequency for all cases. Also note that the other peaks in the transmissibility for Cases B–D occur at slightly different frequencies than for the symmetric case. Peaks corresponding to the first and second peaks of the symmetric case occur at higher frequencies than for the symmetric case, and peaks corresponding to the third peak of the symmetric case occur at lower frequencies than for the symmetric case. Similar behavior was noted for all examples analyzed in Cases B–D [3].

As for the symmetric case, the vibration modes for Cases B–D are analyzed. The first mode for all three cases corresponds to a large vertical displacement of the plate, similar to the first mode for the symmetric case.

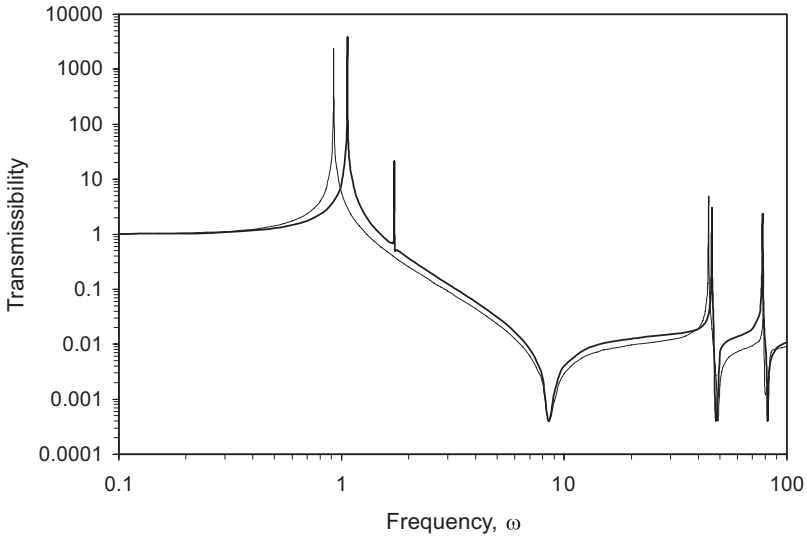

Fig. 8. Transmissibility curves, $0.1<\omega<100$. Dark solid curve, $a_1 = 0.35$, $b_1 = 0.50$, $i_x = 22.11$, $i_y = 27.57$ (Case B) and light solid curve, $a_1 = 0.50$, $b_1 = 0.50$ (Case A).

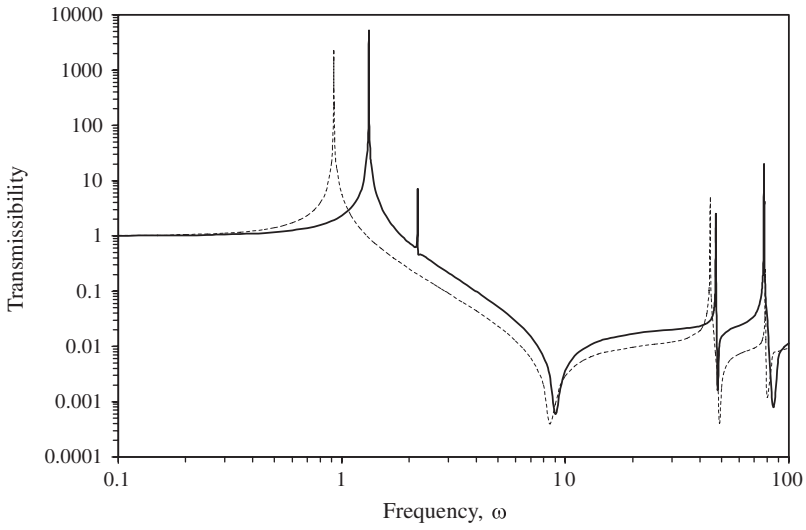

Fig. 9. Transmissibility curves, $0.1<\omega<100$. Dark solid curve, $a_1 = 0.35$, $b_1 = 0.35$, $i_x = 27.57$, $i_y = 27.57$ (Case C) and dashed curve, $a_1 = 0.50$, $b_1 = 0.50$ (Case A).

Because of the eccentric weight in Cases B–D, the plate also rotates slightly in this first mode. At the third peak frequency for Cases B and C and the fourth peak frequency for Case D, the columns in all four isolators vibrate with mode shapes similar to the second mode shape for Case A. At the fourth peak frequency for Cases B and C and the fifth peak frequency for Case D, the columns in all four isolators vibrate with mode shapes similar to the third mode shape for Case A [3].

Upon analysis of the vibration modes at the additional peaks in the transmissibility curves for Cases B–D, it is determined that these peaks correspond to rotational modes for the plate. Nodal lines for examples from Cases B–D are shown in Figs. 11–13, respectively. In these figures, the dot represents the location of the center of mass. Note that these are not pure rotations because the plate exhibits some vertical motion in these modes. Because of this vertical motion, the nodal line shifts slightly during rotation. The lines in Figs. 11–13 represent the nodal lines at the time of maximum rotation.

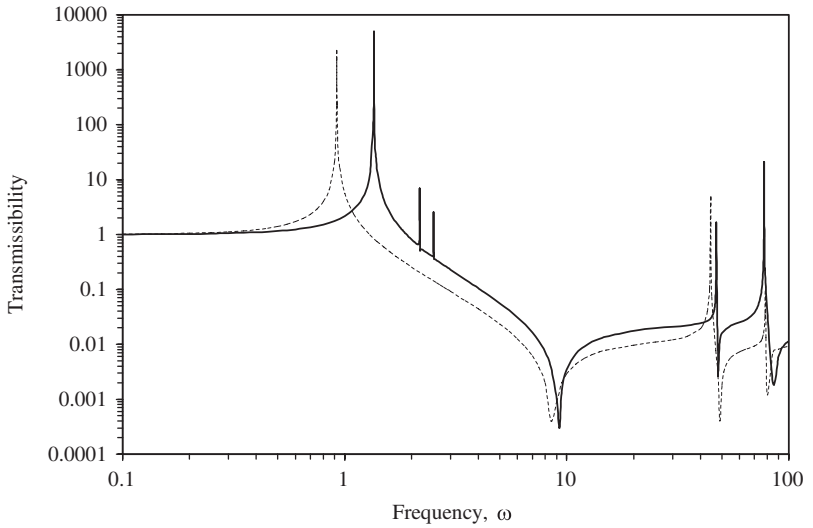

Fig. 10. Transmissibility curves, $0.1<\omega<100$. Dark solid curve, $a_1 = 0.35$, $b_1 = 0.45$, $i_x = 22.72$, $i_y = 27.57$ (Case D) and dashed curve, $a_1 = 0.50$, $b_1 = 0.50$ (Case A).

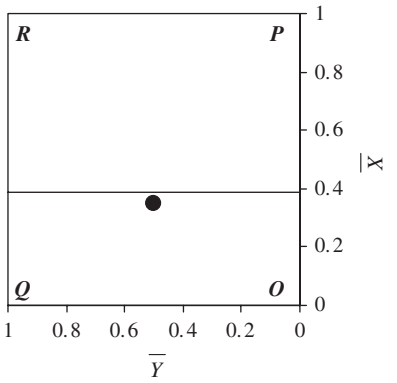

Fig. 11. Nodal line at the second peak frequency, $a_1 = 0.35$, $b_1 = 0.50$ (Case B), $\omega = 1.723$.

For Case B, the nodal line shown in Fig. 11 corresponds to a rotation about a line perpendicular to the line of symmetry. This rotation is similar to rotation about A–A' in Fig. 5(b) that was obtained from the free vibration analysis. For Case C, the nodal line shown in Fig. 12 corresponds to a rotation about a line perpendicular to the line of symmetry. This rotation is similar to rotation about A–A' in Fig. 5(c) that was obtained from the free vibration analysis. For Case D, the two nodal lines shown in Fig. 13 are almost perpendicular to each other. This agrees well with the results from the free vibration analysis.

4. Concluding remarks

Pairs of pre-bent columns bonded with a viscoelastic filler were analyzed as vibration isolators in a system that incorporated 3D motions of the supported mass. The system consisted of a horizontal, rigid plate supported at each corner by a pair of pre-bent columns. Various locations of the plate's center of mass were considered. Free vibrations about equilibrium were examined first, and then the steady-state response of the system to simple-harmonic vertical base displacement was investigated.

Under free vibration, the vibration frequencies and modes of the plate were determined. Under forced vibration, the transmissibility was computed and plotted as a function of the nondimensional excitation

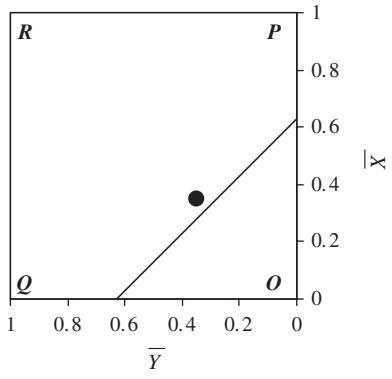

Fig. 12. Nodal line at the second peak frequency, $a_1 = 0.35$, $b_1 = 0.35$ (Case C), $\omega = 2.188$.

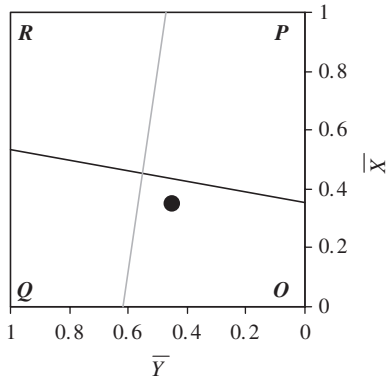

Fig. 13. Nodal lines at the second and third peak frequencies, $a_1 = 0.35$, $b_1 = 0.45$ (Case D). Dark solid line, $\omega = 2.179$; light solid line, $\omega = 2.516$.

frequency for various cases. For the symmetric case, three peaks occurred in the transmissibility over the range of excitation frequencies that was considered. For cases in which the plate's center of mass had some eccentricity, one or two additional peaks were obtained. Analysis of the mode shapes at the additional peaks demonstrated that these peaks corresponded to rotational modes of the plate. The peaks associated with modes that were dominated by vertical plate motion occurred at slightly different frequencies than for the symmetric case. Despite these changes in transmissibility caused by the eccentric center of mass of the plate, the isolators were effective for a significant range of excitation frequencies.

Acknowledgments

This research was supported by the US National Science Foundation under Grant no. CMS-0301084. The authors are grateful to the reviewers for their helpful comments.

References

[1] R.H. Plaut, H.M. Favor, A.E. Jeffers, L.N. Virgin, Vibration isolation using buckled or pre-bent columns, part 1: two-dimensional motions of horizontal rigid bar, *Journal of Sound and Vibration*, doi:10.1016/j.jsv.2007.09.037.

[2] Y.G. Tang, Q. Ding, Y.S. Chen, Vibration control of the platform system with hydraulic supports, *Journal of Vibration and Control* 9 (2003) 1093–1100.

[3] A.E. Jeffers, Vibration Isolation of a Horizontal Rigid Plate Supported by Pre-bent Struts, MS Thesis, Virginia Polytechnic Institute and State University, Blacksburg, VA, 2005 〈http://scholar.lib.vt.edu/theses/available/etd-12192005-145156〉.

[4] S. Wolfram, *The Mathematica Book*, Third ed., Cambridge University Press, Cambridge, UK, 1996.